

Article

# Effect of Overflow Pipe on the Internal Flow Fields and Separation Performance of W-Shaped Hydrocyclones

Lanyue Jiang , Peikun Liu \* , Xinghua Yang, Yuekan Zhang, Xiaoyu Li, Yulong Zhang and Hui Wang

College of Mechanical & Electronic Engineering, Shandong University of Science and Technology, Qingdao 266590, China; jianglanyue5@163.com (L.J.); yxh19781025@126.com (X.Y.); zhangyk2007@163.com (Y.Z.); lixy2018@sdust.edu.cn (X.L.); yulong\_89@126.com (Y.Z.); wang\_hui\_1992@163.com (H.W.)

\* Correspondence: lpk710128@163.com; Tel.: +86-0532-8605-7176

Received: 19 February 2020; Accepted: 5 April 2020; Published: 7 April 2020



**Abstract:** The entrainment of fine particles in underflow of a grinding-classification hydrocyclone can cause ore overgrinding, which will lead to reductions in both metal recovery and ball mill throughput. To address this problem, this paper proposed a W-shaped hydrocyclone that can effectively reduce underflow fine particle entrainment. Experimental tests and numerical simulations were employed to deeply investigate overflow pipe diameter influence on the separation performance and internal flow field of W-shaped hydrocyclones. The effects of overflow pipe diameter on air core shape, velocity field, pressure field, and separation performance were studied. The results revealed that as the diameter of the overflow pipe increased, air core gradually stabilized, and air core diameter gradually increased. The diameter of stabilized air core was approximately 45% to 55% of overflow pipe diameter. As overflow pipe diameter increased, hydrocyclone pressure drop decreased, energy consumption was reduced, the tangential velocity decreased, outer vortex axial velocity did not change significantly, and inner vortex axial velocity gradually increased. At the same time, zero-velocity points gradually moved outward, and the inner vortex region expanded. By the increase of overflow pipe diameter, both the underflow yield and split ratio gradually decreased, the coarse particle content in the overflow product increased, and the fine particle content in the underflow product gradually decreased.

**Keywords:** W-shaped hydrocyclone; CFD; experimental study; flow field; separation performance

## 1. Introduction

The hydrocyclone has been widely used as a classification and separation device in grinding-classification operations. However, hydrocyclone classification can result in “fish-hook” (fine particle entrainment in underflow) and coarse particles in overflow, a phenomenon known as derichment [1–4]. In the classification of high-concentration coarse-grained materials, the “fish-hook” depends on the settling velocity of multi-component particles in a swirling flow field. This derichment often causes ore over-grinding, which leads to further problems, such as reductions in the metal recovery and the ball mill throughput. Therefore, the prevention of “fish-hook” has become an active and challenging research topic [5–8].

To address the above problem, many scholars have conducted studies to optimize the hydrocyclone structure. Dueck [9–11] injected clean water at a certain location in the cone section at a specific speed to disperse the outer swirl, pushing the fine particles settled on cyclone wall towards its center, making them re-enter the inner swirl and discharge from the overflow port to reduce the amount of

fine particles which enter the underflow. Vieira [12,13] proposed a filtering hydrocyclone, in which a conical filtering wall replaced a conical section. The conical filtering wall had extremely small pores. Fine particles could pass through the conical filtering wall, while large particles could not. Finally, three products were obtained: the overflow, the underflow, and the filtrate. Ghodrati [14,15] studied the configuration of the hydrocyclone conical section. The shape and length of the conical section of the hydrocyclone were investigated using the numerical method. A cone configuration suitable for different situations was obtained. Yang [16,17] used CFD (Computational Fluid Dynamics) to compare the separation performances of the traditional single-cone hydrocyclone and a double-cone hydrocyclone. The double-cone cyclone improved the separation efficiency and sharpness compared to that of the traditional design. Jiang et al. [18,19] carried out a detailed study to show that there were fewer fine particles in the underflows of hydrocyclones with parabolic cones, than in traditional hydrocyclones. To overcome ultrafine particle classification problems in traditional hydrocyclones, Ye et al. [20] investigated the cross-section of a conical section and designed a multi-section composite cone. In our previous research, a new type of W-shaped hydrocyclone (Figure 1) was proposed to address the problem of “fish-hook” [21]. The results showed that the W-shaped structure could effectively reduce “fish-hook”. However, structural parameters, operating parameters, and physical property parameters all have important effects on the W-shaped hydrocyclones. Therefore, further research on W-shaped hydrocyclones is needed.

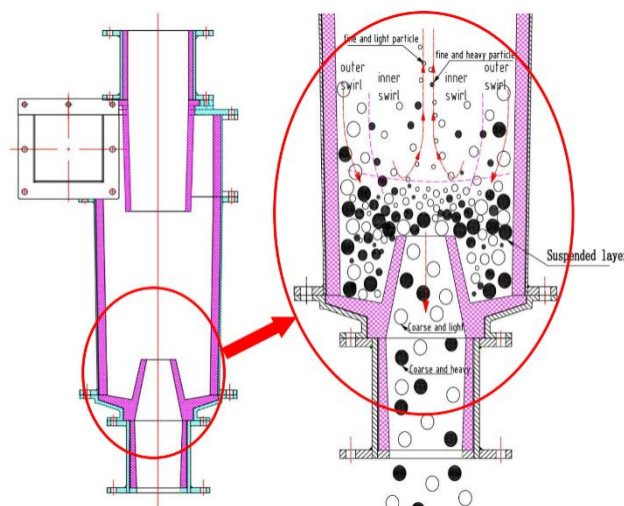


**Figure 1.** W-shaped full cylindrical hydrocyclone.

Currently, hydrocyclone flow field parameters can be accurately measured by experimental methods. However, experimental methods also have limitations. When measuring different flow field parameters, various structural components must be manufactured and different measurement methods must be performed. The labor, material, and time costs are huge [22–24]. With technological progress, CFD has become a powerful method for the simulation of complex flow phenomena. Almost all flow field parameters can be obtained at the same time by CFD [25–29]. Cui et al. [30,31] investigated the flow field and air core characteristics with water-only condition by using the RSM (Reynolds Stress Model) and VOF (Volume of Fluid), and it showed a good agreement between simulation and PIV measurement results. Delgadillo and Rajamina [32,33] developed and simulated six 75 mm hydrocyclones with different cone angles and cylindrical geometries. They used RSM and LES (Large Eddy Simulation) models in combination with the VOF model to study air core, and in combination with the DPM (Discrete Phase Model) model to study the particle trajectory. Narasimha [34,35] used the same models to study velocity distribution in hydrocyclones, and the results showed that both models have higher accuracy. Jiang et al. [36] used the Euler model to simulate a two-stage series hydrocyclone and obtained the flow field distribution and classification performance. Zhang et al. described the

turbulence characteristics of a gas-liquid two-phase flow with the RSM model and simulated particle motion with the DPM model. The forces on the particles were obtained by numerical simulation. The spatial and statistical distributions of the particles were analyzed. Chu et al. [37,38] used the CFD method to solve the continuous phase and used the DEM (Discrete Element Method) method to solve the discrete phase. Particle density effect on hydrocyclone separation performance was explored by combining the two methods. Slack et al. [39,40] employed RSM and LES models for the simulation of the turbulent field inside a 205 mm hydrocyclone and compared the obtained tangential and axial velocities with LDV (Laser Doppler Velocimetry) test data. They showed that the results obtained from the RSM turbulence model agreed well with those of the LDV tests and required lower mesh quality and computational cost.

For specific engineering problems, the study of the factors affecting the hydrocyclone separation performance will provide a significant reference for optimizing hydrocyclone design. Therefore, in this work, experimental tests and numerical simulations were combined for the investigation of overflow pipe diameter effect on the internal flow field and classification performance of W-shaped hydrocyclones.

## 2. Methods

Flow field distribution in W-shaped hydrocyclones, including air core, velocity field, and pressure field, were obtained through numerical simulations. Then, the separation performance of the hydrocyclone was obtained by experimental tests, including solid phase yield, split ratio, cut size, and efficiency.

### 2.1. Numerical Simulation

#### 2.1.1. Model Validation and Meshing

Figure 2 shows the structure of a W-shaped hydrocyclone. A Cartesian coordinate system was considered with its origin at the center of apex, feed direction as the positive x-axis direction, and overflow pipe direction as the positive z-axis direction.

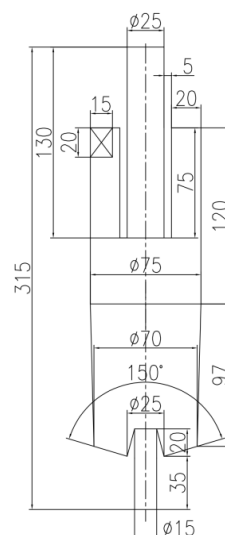


**Figure 2.** Structure of W-shaped hydrocyclone.

Figure 3 shows the meshes applied in simulations. Mesh division is an important part of numerical simulation preprocessing. The type, quality and number of grid cells highly affect the speed and accuracy of simulations. Due to relatively simple hydrocyclone fluid domain structure, a hexahedral mesh is used, which has the advantages of high calculation accuracy and fast speed. Grid independence check needs to be performed to ensure calculation accuracy and improve calculation efficiency. The results have been shown in previous studies and will not be included here [21]. To facilitate the analysis of the

flow field, the characteristic sections  $Z = 75$ ,  $Z = 100$ ,  $Z = 125$ , and  $Z = 175$  were selected for analysis, as shown in Figure 4.

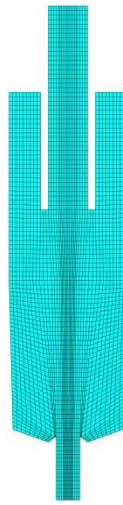


Figure 3. The Mesh.

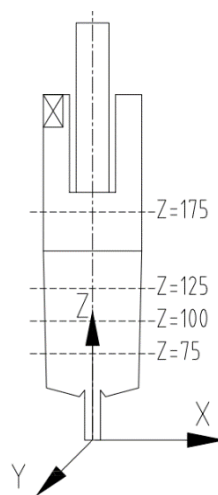


Figure 4. Characteristic sections.

### 2.1.2. Simulation Conditions

W-shaped hydrocyclone flow field was obtained by the RSM and VOF models. The “velocity-inlet” boundary condition was used at the hydrocyclone inlet. Liquid phase velocity was 5 m/s. The boundary condition of the outlet was assumed to be a “pressure-outlet”. In the VOF model, the volume fraction of air backflow was assumed to be 1, so that the simulation could create an air core by drawing air from both outlets due to central negative pressure. No-slip boundary condition was assumed for hydrocyclone walls, and standard wall function method was applied for the calculation of turbulence performance near the wall surface. For pressure-velocity coupling, the SIMPLE algorithm was applied, pressure equations were obtained using PRESTO discretization scheme, and other control equations were derived using QUICK discretization scheme. Flow rate time-averaged equilibria for each phase, at both inlet and outlet, were taken as convergence criteria. Fixed time steps of  $1.0 \times 10^{-4}$  s were applied in all cases.

## 2.2. Experimental

### 2.2.1. Experimental Equipment

A hydrocyclone separation test system was designed to determine the separation performance of a  $\Phi 75$  mm W-shaped hydrocyclone. The system mainly consisted of a mixing tank, pump, pipelines, valves, pressure gauges, flow meters, frequency converter, and a hydrocyclone, as shown in Figure 5. Closed-circuit operation was adopted to facilitate sampling and observation in the experiment. First, materials of prescribed concentrations were prepared. The materials were evenly mixed in a mixing tank and fed into the hydrocyclone through a slurry pump to complete the separation process. The underflow and overflow products were re-introduced into the mixing tank. The pump flow was adjusted by a frequency converter to a specified feed pressure. The W-shaped hydrocyclone is shown in Figure 6. After the test parameters were determined, the system was kept running stably for a prescribed period of time. The experimental error was reduced by multiple sampling and comparison of the results. After the system stabilized, prescribed amounts of the separated products were collected from the recirculation line, the apex, and the overflow pipe. The mass concentrations of the feed, the overflow product, and the underflow product were measured by drying and weighing methods. Particle size composition was determined by a BT-9300S laser particle size analyzer. Performance indicators, such as the yield and efficiency, were calculated and analyzed.

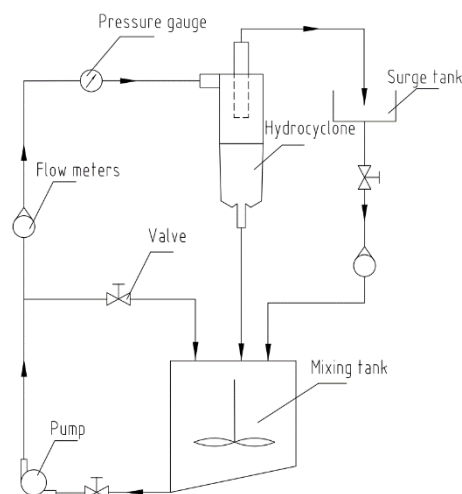


Figure 5. Hydrocyclone separation performance test set-up.



Figure 6. W-shaped hydrocyclone.

### 2.2.2. Materials

To eliminate the errors caused by the separation effect, quartz powder with 98% purity (with  $\text{SiO}_2$  as the main component) was used in this study. The density of the quartz powder was  $2650 \text{ kg/m}^3$ . Table 1 and Figure 7 show the particle size composition and distribution curve, respectively. Particles smaller than  $23 \mu\text{m}$  accounted for 28.27% of the total particles, particles smaller than  $45 \mu\text{m}$  accounted for 50.21%, and particles larger than  $100 \mu\text{m}$  accounted for 13.92%. As the cut size of the 75 mm hydrocyclone was  $25\text{--}75 \mu\text{m}$ , this material was suitable for testing the separation performance of the W-shaped hydrocyclone. Particles smaller than  $23 \mu\text{m}$  were defined as fine particles, while particles larger than  $100 \mu\text{m}$  were defined as coarse particles.

**Table 1.** Particle size composition of test material.

Mesh Number	Size/ $\mu\text{m}$	Content/%	Negative Accumulation/%	Positive Accumulation/%
<60	>250	0.04	100	0.04
60–70	212–250	0.32	99.96	0.36
70–80	180–212	0.99	99.64	1.35
80–100	150–180	2.73	98.65	4.08
100–140	109–150	9.84	95.92	13.92
140–200	75–100	13.94	86.08	27.86
200–325	75–45	21.93	72.14	49.79
325–600	23–45	21.94	50.21	71.73
600–1250	10–23	15.61	28.27	87.34
>1250	<10	12.66	12.66	100

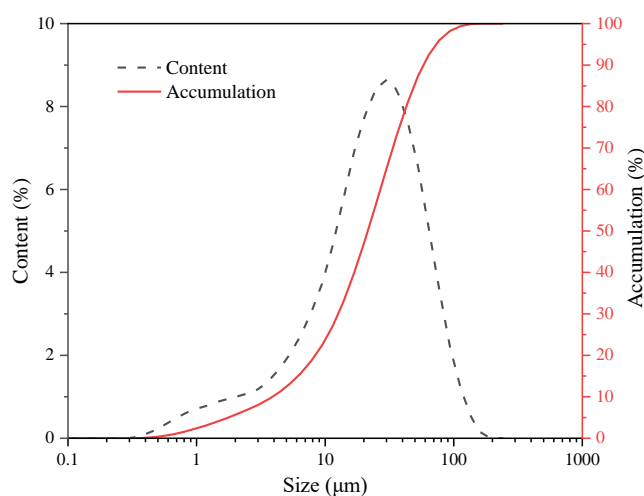


**Figure 7.** Particle size distribution of test material.

### 2.2.3. Performance Index

The ratio underflow to overflow volume flow rates is defined as split ratio, which is used to represent the flow distribution relationship between overflow and underflow. Equation (1) shows the calculation formula.

$$f = \frac{V_u}{V_o}, \quad (1)$$

where  $V_u$  and  $V_o$  are underflow and overflow volume flow rates, respectively.

The solid-phase yield is the ratio of solid-phase mass flow rate of underflow to that of the feed inlet. This solid phase mass flow rate includes the mass flow rates of all solid particles of different particle sizes, which is used to characterize the total recovery rate of solid phase particles from the underflow. The calculation formula is shown in Equation (2).

$$\gamma = \frac{M_u}{M_i} \times 100\%, \quad (2)$$

where  $M_u$  and  $M_i$  are underflow and inlet solid-phase mass flow rates, respectively.

Quantity efficiency is defined as the amount of solid phase particles with a specific size entering the overflow product, which is used to characterize the recovery rate of the overflow product to specific particle sizes. The calculation formula is shown in Equation (3).

$$F = \frac{M_o f_o(d)}{M_i f_i(d)} \times 100\%, \quad (3)$$

where  $f_o(d)$   $f_i(d)$  are the contents of a specific particle in overflow and feed inlet, respectively.  $M_o$  is the solid-phase mass flow rate of the overflow.

For the evaluation of hydrocyclone separation performance, the quantity index of underflow recovery yield and the quality index of a specific particle content should be considered, so the concept of quality efficiency is introduced. The calculation formula is shown in Equation (4).

$$E = \frac{100(\beta - \alpha)(\alpha - \theta)}{\alpha(100 - \alpha)(\beta - \theta)} \times 100\%, \quad (4)$$

where  $\alpha$  is the cumulative content of a specific particle in feed inlet,  $\beta$  is the cumulative content of a specific particle in overflow, and  $\theta$  is the cumulative content of a specific particle in underflow.

### 3. Results and Discussion

#### 3.1. Flow Field Analysis

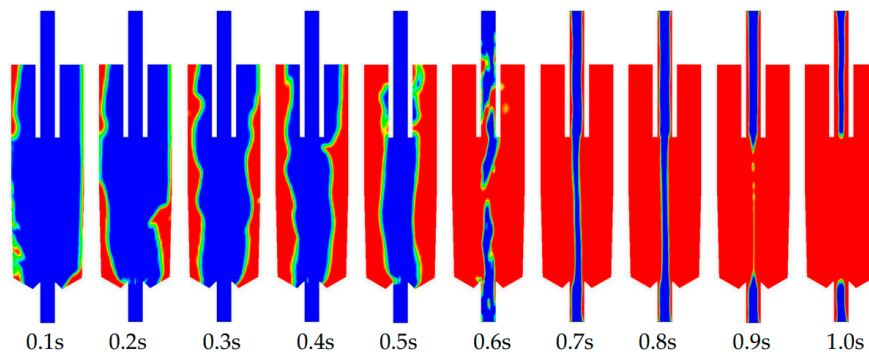
The overflow pipe is the outlet of fine-grained materials during the classification process. Approximately 80% of the slurry is discharged from the overflow pipe. Overflow pipe diameter significantly affects hydrocyclone separation performance. Therefore, the effect of overflow pipe diameter must be investigated. Here, overflow pipe diameter was chosen to be 15, 20, 25, 30, and 35 mm, which were 20% to 47% of the diameter of the main body of the hydrocyclone.

##### 3.1.1. Effect on Air Core

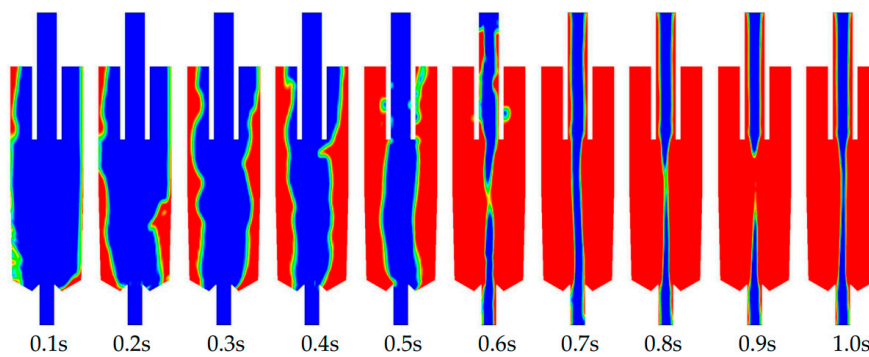
Overflow pipe diameter effect on air core is analyzed in Figure 8. The red part shows liquid phase, the blue part shows gas phase, and the green area shows gas-liquid interface. We found that overflow pipe diameter had a significant effect on air core formation. When overflow pipe diameter was 15 mm (apex diameter of 15 mm), the water-filling process was the same as in the conventional process. A full air core was formed at approximately 0.7 s and then gradually disappeared. At approximately 1 s, the air core existed only inside the overflow pipe and the apex. At overflow pipe diameter of 20 mm, air core first stabilized at approximately 0.7 s and then gradually disappeared. At approximately 1 s, the air core was formed again and just barely extended through the hydrocyclone. When the overflow pipe diameter was increased to more than 25 mm, a relatively stable air core was formed. With the increase of overflow pipe diameter, air core diameter increased significantly, and the air core stability was improved.

Figure 9 shows air core diameter and position. The diameter of the air core in overflow pipe was used as a reference for comparison. With the increase of overflow pipe diameter from 20 to 35 mm, air core diameter increased from 9.16 to 18.96 mm. When the overflow pipe diameter was 20, 25, 30, and 35 mm, the proportion of the corresponding air core diameter to the overflow pipe diameter was 0.458, 0.5, 0.5, and 0.54, respectively. The air core generated inside the hydrocyclone increased with increasing overflow pipe diameter. When the diameter of the overflow pipe increased to a certain extent, the enlarged air core greatly occupied the discharge area of the apex. At overflow pipe diameter

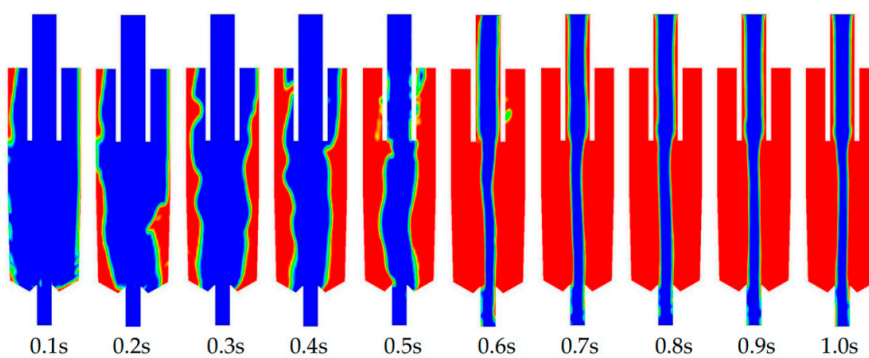
of 35 mm, air core diameter inside the apex was as high as 14.32 mm. Since the diameter of the apex was only 15 mm, the air core occupied more than 90% of the discharge area.



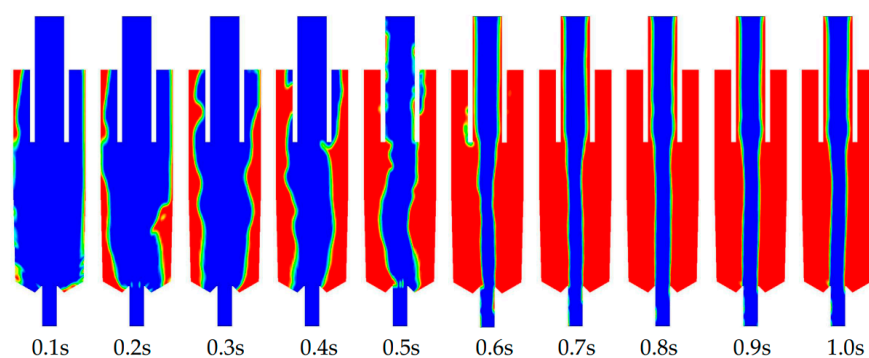
(a) Overflow pipe diameter of 15 mm



(b) Overflow pipe diameter of 20 mm

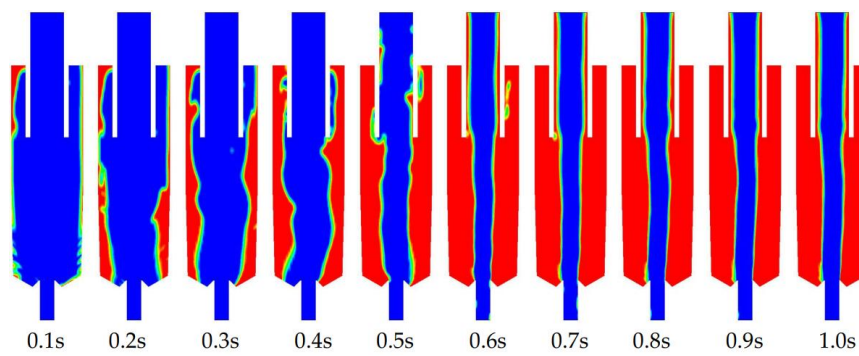


(c) Overflow pipe diameter of 25 mm



(d) Overflow pipe diameter of 30 mm

Figure 8. Cont.



(e) Overflow pipe diameter of 35 mm

Figure 8. Air core formation.

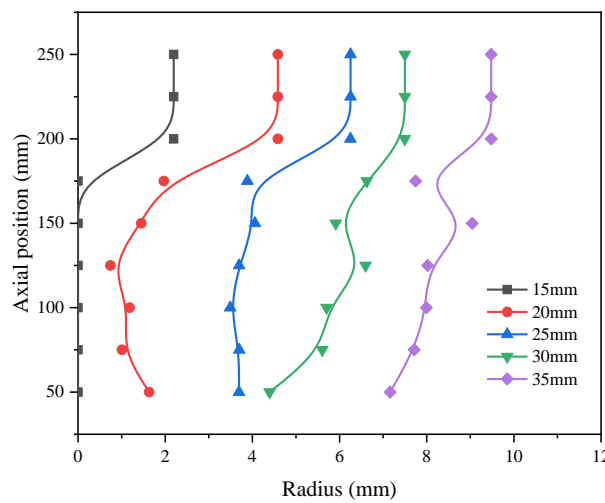


Figure 9. The air core diameter.

### 3.1.2. Effect on Pressure Drop

The air core occupies the forced vortex region of the hydrocyclone and has a significant impact on the energy dissipation. It can be seen from the above discussion that overflow pipe diameter significantly affects air core. Therefore, air core diameter effect on pressure drop was analyzed. Figure 10 shows the obtained results. Pressure drop decreased significantly when increasing the diameter of the overflow pipe. With the increase in overflow pipe diameter from 15 to 35 mm, the pressure drop was reduced from 164,202.08 Pa to 53,048.82 Pa, which was a decrease of 67.69%. Overflow pipe diameter effect on pressure drop was significant. Increasing overflow pipe diameter is an effective method to decrease energy consumption and increase hydrocyclone throughput. Figure 11 shows overflow pipe diameter effect on radial pressure distribution in W-shaped hydrocyclones. A comparison of the pressure distribution at each axial location showed that the change in radial pressure drop was consistent with that of the total pressure drop. The radial pressure drop decreased with the increase of overflow pipe diameter.

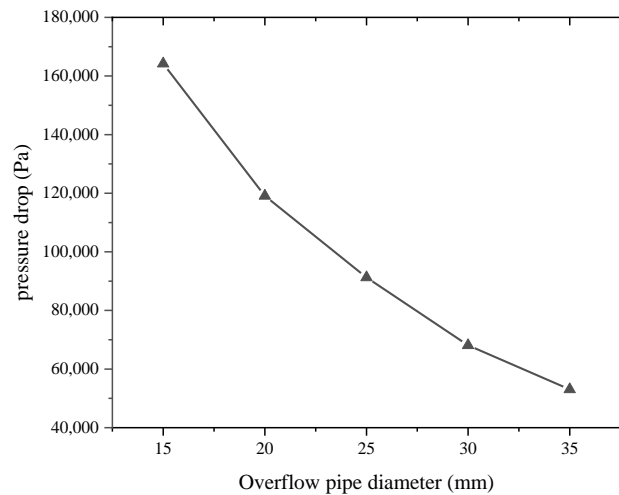


Figure 10. The pressure drop.

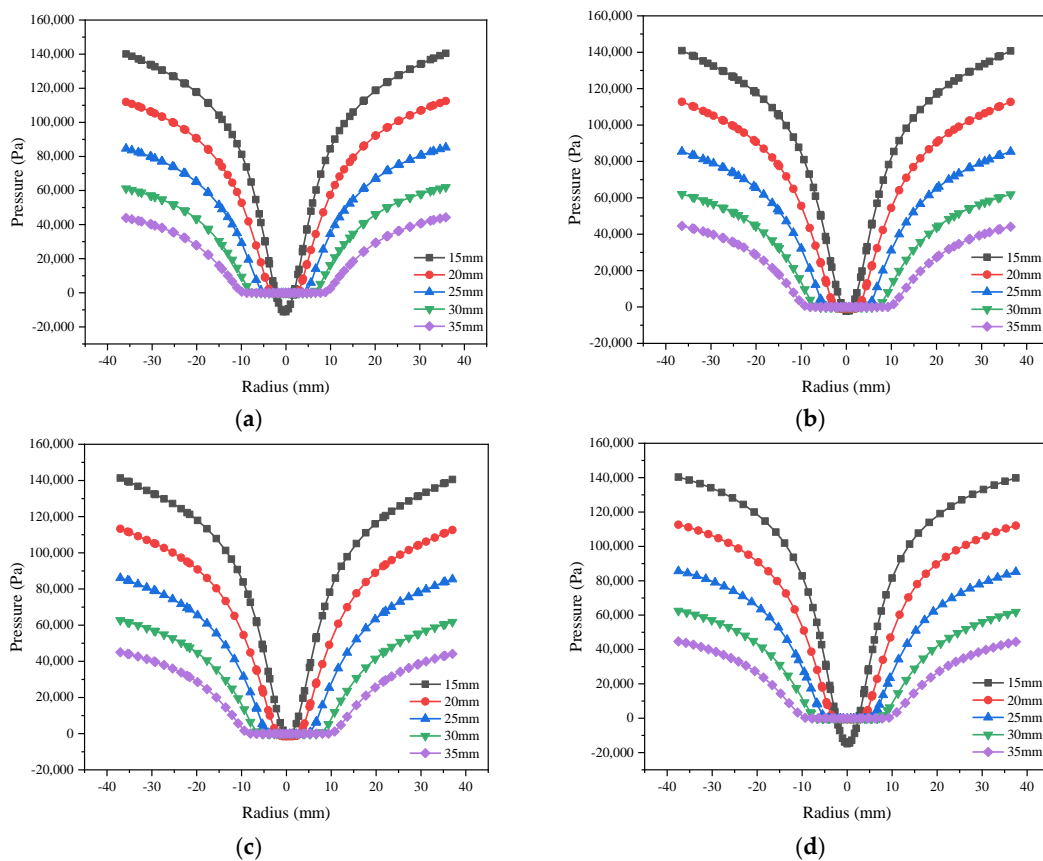


Figure 11. The radial pressure distribution: (a)  $Z = 75$ ; (b)  $Z = 100$ ; (c)  $Z = 125$ ; (d)  $Z = 175$ .

### 3.1.3. Effect on Tangential Velocity

The effect of overflow pipe diameter on tangential velocity in W-shaped hydrocyclones is shown in Figure 12. Tangential velocity obviously reduced as overflow pipe diameter increased. Taking the cross section of  $Z = 100$  as an example, as the diameter of overflow pipe increased from 15 to 35 mm, maximum tangential velocity was reduced from 8.15 m/s to 6.64 m/s. We also found that the maximum tangential velocity track gradually moved outward as the overflow pipe diameter increased. The maximum tangential velocity track forms a boundary between the forced vortex and quasi-free vortex. Therefore, when the diameter of the overflow pipe was increased, the inner forced vortex

region expanded, and the outer quasi-free vortex region shrank. This trend was also directly related to the expansion of the air core.

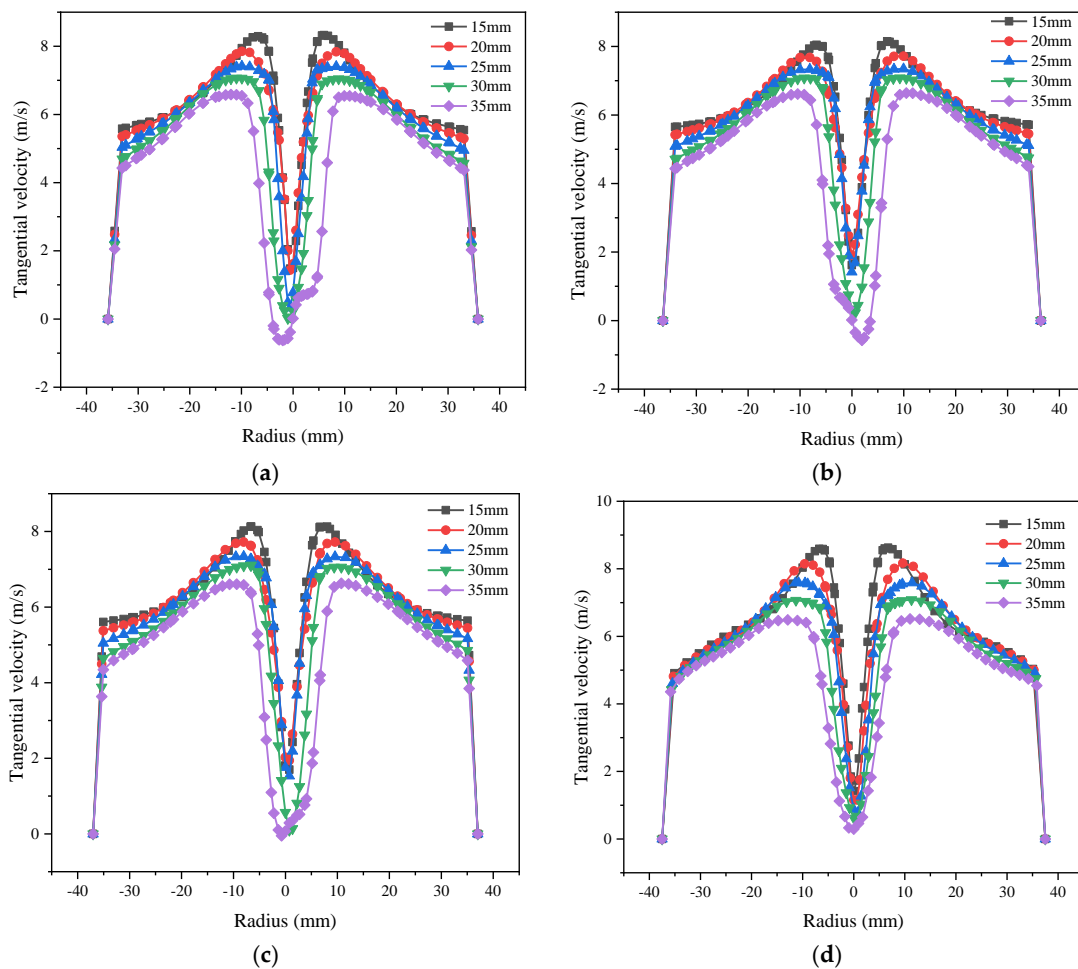
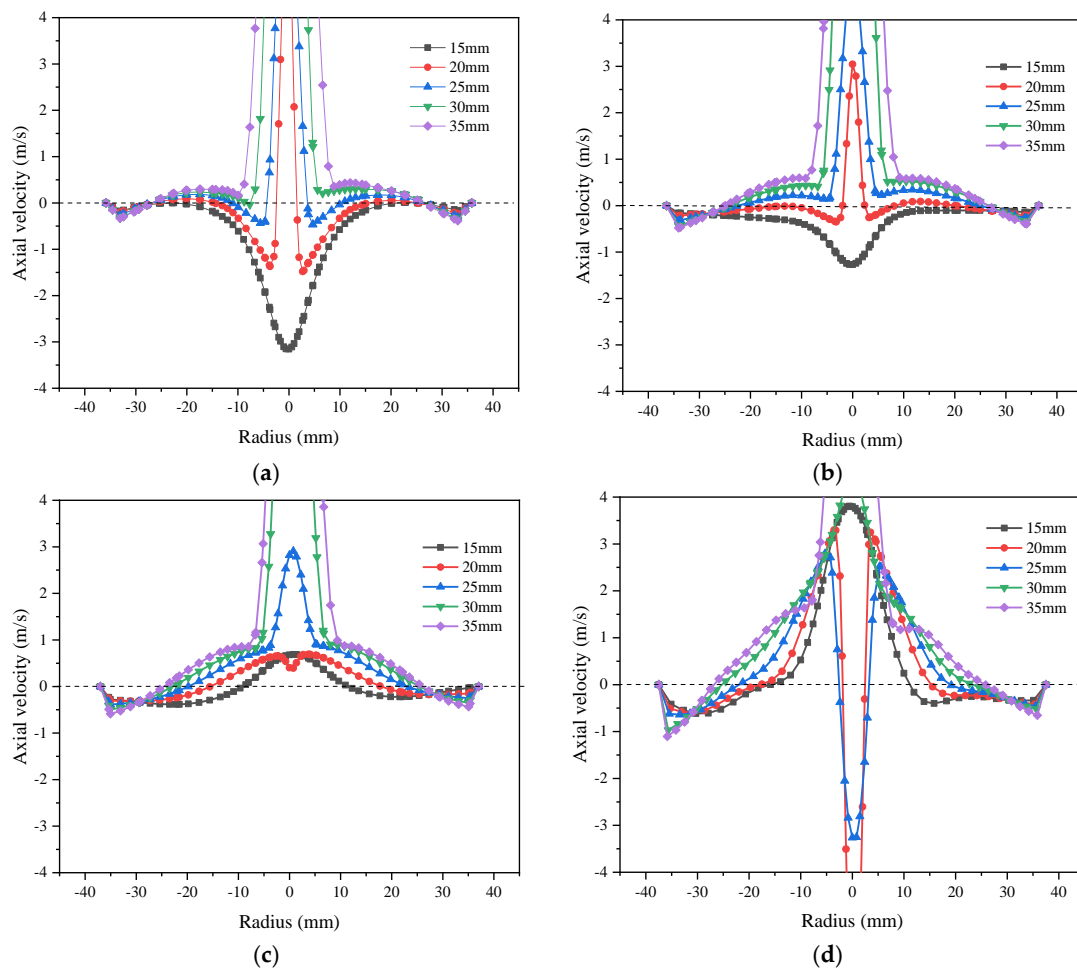


Figure 12. The tangential velocity: (a) Z = 75; (b) Z = 100; (c) Z = 125; (d) Z = 175.

### 3.1.4. Effect on Axial Velocity

Figure 13 shows the overflow pipe diameter effect on axial velocity. Overflow pipe diameter had little effect on outer vortex axial velocity in the main separation zone but had a significant effect on inner vortex axial velocity. Upward axial velocity gradually increased with the increase of the diameter of overflow pipe. On the Z = 175, Z = 125, and Z = 100 cross sections, it was found that as the overflow pipe diameter increased, the zero-velocity points gradually moved outward; i.e., upward inner vortex region expanded, and downward outer vortex region shrank. The overflow flow gradually increased, which was the main reason for the decrease in split ratio with the increase of overflow pipe diameter. Especially at an overflow pipe diameter of 15 mm, it could be found from the two cross sections of Z = 75 and Z = 100 that the axial velocities were all negative and the fluid was completely discharged from the underflow, which was the reason why split ratio was as high as 50% or more. Therefore, in the actual application process, the overflow pipe should not be too small, and a full air core should be used as an evaluation indicator of the normal separation process.



**Figure 13.** The axial velocity: (a)  $Z = 75$  (b)  $Z = 100$ ; (c)  $Z = 125$ ; (d)  $Z = 175$ .

### 3.2. Analysis of Separation Performance

With gradual increase in the overflow pipe diameter from 15 mm to 30 mm, underflow yield monotonically decreased from 61.39% to 8.58%, and split ratio monotonically decreased from 44.6% to 4.6% (Figure 14). The overflow pipe diameter greatly affected underflow yield and split ratio. Combined with the simulation analysis of flow field, the reason for this phenomenon was described as follows: when overflow pipe diameter increased, not only did the upward axial velocity gradually increase, the inner vortex region also expanded. Thus, the amounts of the solid phase and liquid phase entrained in the underflow were both reduced.

Figure 15 shows the change in the product concentration. Both underflow and overflow concentrations increased by increasing the diameter of the overflow pipe. Overflow concentration increased from 11.99% to 18.56%, an increase of 54.79%; the underflow concentration increased from 32.43% to 45.9%, an increase of 41.53%. Combined with the trends of the split ratio and yield, it can be known that for the overflow product, the increase in the liquid phase content was smaller than that of the solid phase content; for the underflow product, the decrease in the liquid phase content was greater than that of the solid phase content.

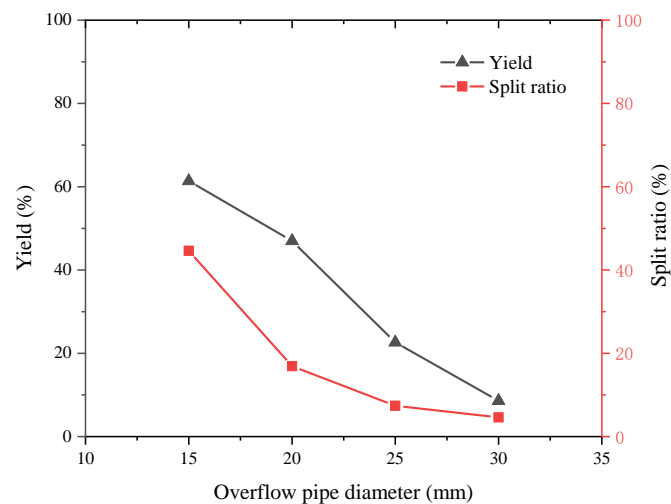


Figure 14. The yield and split ratio.

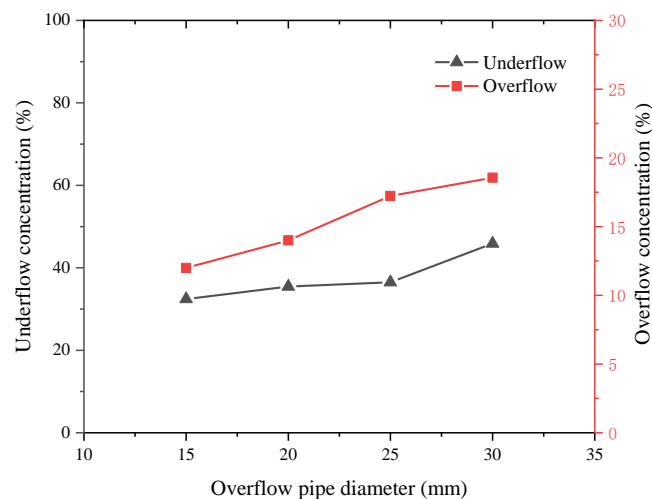


Figure 15. The product concentration.

Figure 16 shows, that as overflow pipe diameter increased, both overflow and underflow products became coarser. In the overflow, the content of the  $-25\ \mu\text{m}$  particles decreased from 47.09% to 31.94%, while the content of the  $+100\ \mu\text{m}$  particles increased from 3.04% to 14.31%; in the underflow, the content of the  $-25\ \mu\text{m}$  particles decreased from 15.03% to 7.39%, while the content of the  $+100\ \mu\text{m}$  particles increased from 34.34% to 51.78%. Part of the reason for this phenomenon was the change in the split ratio. In addition, with the increase of overflow pipe diameter, centrifugal force field was weakened, tangential velocity decreased, and some particles could no longer overcome the fluid resistance to enter the underflow.

Figure 17 shows overflow pipe diameter effect on the classification efficiency curve. Overflow pipe diameter had a great effect on hydrocyclone classification performance. As overflow pipe diameter increased, the classification efficiency curve shifted to the right significantly, and the recovery of all particle sizes to underflow were greatly reduced. At an overflow pipe diameter of 15 mm, the recovery of fine particles in the underflow exceeded 25%, which indicated the “fish-hook”; at an overflow pipe diameter of 30 mm, coarse particles were not all recovered by the hydrocyclone, which indicated serious coarse particles entrainment in overflow. The simulation showed, that at very large overflow pipe diameters, the air core formed by the hydrocyclone occupied most of the space in the apex, which seriously affected the underflow discharge. As a result, the underflow yield and split ratio were both small.

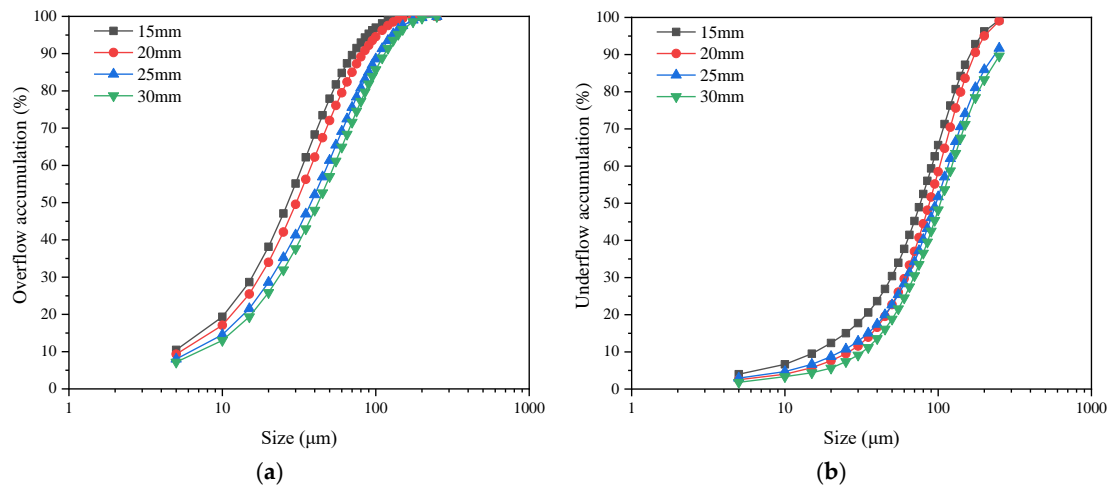


Figure 16. The product particle size: (a) Overflow particle size; (b) Underflow particle size.

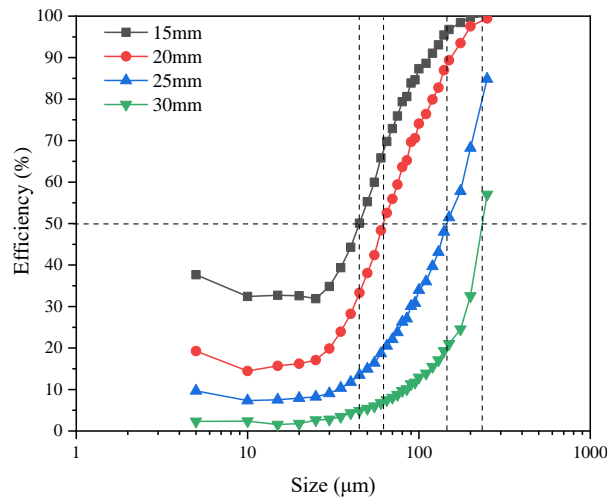


Figure 17. The classification efficiency curve.

The rightward shift of the classification efficiency curve indicated an increase in cut size. With the increase of overflow pipe diameter from 15 to 30 mm, the cut size sharply increased from 45  $\mu\text{m}$  to 236  $\mu\text{m}$ . It was known from Table 2 that as the overflow pipe diameter increased, the classification effectiveness gradually decreased, while the quantity efficiency gradually increased. At an overflow pipe diameter of 30 mm, although quantity efficiency was as high as 98.57%, the quality efficiency was only 6.44%. Therefore, although increasing the overflow pipe diameter can reduce the fine particle entrainment in the underflow to a certain extent, it is not desirable. If the overflow pipe diameter exceeds a certain limit, the coarse particle entrainment in the overflow will become very serious, and the quality efficiency will be severely reduced.

Table 2. The classification performance.

Overflow Pipe Diameter/mm	Cut Size/ $\mu\text{m}$	Content of $-25 \mu\text{m}$ Particles/%		Quality Efficiency/%	Quantity Efficiency/%
		Overflow	Underflow		
15	45	47.09	15.03	37.77	74.48
20	62	42.11	9.50	35.29	88.90
25	144	35.22	10.76	18.00	93.18
30	236	31.94	7.39	6.44	98.57

#### 4. Conclusions

In this study, CFD numerical simulations and experimental tests were employed to investigate a W-shaped hydrocyclone. Overflow pipe diameter effects on air core shape, velocity field, pressure field, and separation performance were evaluated. The following conclusions were drawn:

(1) The diameter of the overflow pipe had a significant effect on the air core. When overflow pipe diameter was too small, the hydrocyclone could not form a stable air core. As the overflow pipe diameter increased, the air core gradually stabilized and the air core diameter gradually increased. Stabilized air core diameter was approximately 45% to 55% of the overflow pipe diameter.

(2) With the increase of overflow pipe diameter, the pressure drop of the hydrocyclone decreased, and the energy consumption was reduced. Increasing the overflow pipe diameter was an effective method to increase throughput. With the increase of overflow pipe diameter, tangential velocity decreased, and maximum tangential velocity track gradually moved outward, which indicated that the inner forced vortex region expanded, and the outer quasi-free vortex region shrank.

(3) Increasing the overflow pipe diameter had little effect on outer vortex axial velocity, but a significant effect on inner vortex axial velocity. Upward axial velocity gradually increased as overflow pipe diameter increased. The zero-velocity points gradually moved outward as the overflow pipe diameter increased, which indicated the expansion of the upward inner vortex region and shrinkage of the downward outer vortex region. The overflow flow gradually increased, which was the main reason why split ratio decreased as overflow pipe diameter increased.

(4) With the increase of overflow pipe diameter, both underflow yield and split ratio gradually decreased, fine particle content of underflow gradually decreased and coarse particle content of overflow product increased. Although increasing the overflow pipe diameter can reduce the entrainment of fine particles in the underflow to a certain extent, it is not desirable. If the overflow pipe diameter exceeds a certain limit, the entrainment of coarse particles in overflow will become very serious, and the quality efficiency will be severely reduced.

**Author Contributions:** Conceptualization, P.L. and L.J.; methodology, L.J.; software, X.Y. and X.L.; validation, Y.Z. (Yuekan Zhang), X.L. and Y.Z. (Yulong Zhang); formal analysis, Y.Z. (Yulong Zhang); investigation, L.J.; resources, P.L.; data curation, X.Y.; writing—original draft preparation, L.J.; writing—review and editing, L.J. and Y.Z. (Yuekan Zhang); visualization, H.W.; supervision, P.L.; project administration, L.J.; funding acquisition, P.L. All authors have read and agreed to the published version of the manuscript.

**Funding:** This work was supported by the National Key R&D Program of China (grant number: 2018YFC0604702) and Shandong Provincial Key Research and Development Program, China (grant number: 2019GSF109030).

**Conflicts of Interest:** The authors have declared no conflict of interest.

#### References

1. Cilliers, J.J.; Harrison, S.T.L. Yeast flocculation aids the performance of yeast dewatering using mini-hydrocyclones. *Sep. Purif. Technol.* **2019**, *209*, 159–163. [[CrossRef](#)]
2. Lv, W.J.; Huang, C.; Chen, J.Q.; Liu, H.L.; Wang, H.L. An experimental study of flow distribution and separation performance in a UU-type mini-hydrocyclone group. *Sep. Purif. Technol.* **2015**, *150*, 37–43. [[CrossRef](#)]
3. Song, T.; Tian, J.Y.; Ni, L.; Shen, C.; Yao, Y. Experimental study on performance of a de-foulant hydrocyclone with different reflux devices for sewage source heat pump. *Appl. Therm. Eng.* **2019**, *149*, 354–365. [[CrossRef](#)]
4. Wu, S.E.; Hwang, K.J.; Cheng, T.W.; Hung, T.C.; Tung, K.L. Effectiveness of a hydrocyclone in separating particles suspended in power law fluids. *Powder Technol.* **2017**, *320*, 546–554. [[CrossRef](#)]
5. Tavares, L.M.; Souza, L.L.G.; Lima, J.R.B.; Possa, M.V. Modeling classification in small-diameter hydrocyclones under variable rheological conditions. *Miner. Eng.* **2002**, *15*, 613–622. [[CrossRef](#)]
6. Botha, S.; Le, R.J.D.; Craig, I.K. Hybrid non-linear model predictive control of a run-of-mine ore grinding mill circuit. *Miner. Eng.* **2018**, *123*, 49–62. [[CrossRef](#)]
7. Zhu, G.F.; Liow, J.L. Experimental study of particle separation and the fishhook effect in a mini-hydrocyclone. *Chem. Eng. Sci.* **2014**, *111*, 94–105. [[CrossRef](#)]

8. Xu, Y.; Wang, H.; Wang, Z.; Fang, Y.; Liu, Y.; Zeng, T.; Liu, Z.; Liu, M. Hydrocyclone breakage of activated sludge to exploit internal carbon sources and simultaneously enhance microbial activity. *Process Saf. Environ. Prot.* **2018**, *117*, 651–659. [[CrossRef](#)]
9. Dueck, J.; Pikushchak, E.; Minkov, L.; Farghaly, M.; Neesse, T. Mechanism of hydrocyclone separation with water injection. *Miner. Eng.* **2010**, *23*, 289–294. [[CrossRef](#)]
10. Wang, H.; Fu, P.; Li, J.; Huang, Y.; Zhao, Y.; Jiang, L.; Fang, X.; Yang, T.; Huang, Z.; Huang, C. Separation-and-Recovery Technology for Organic Waste Liquid with a High Concentration of Inorganic Particles. *Engineering* **2018**, *4*, 406–415. [[CrossRef](#)]
11. Zhang, Y.; Liu, P.; Zhang, Y.; Yang, X.; Jiang, L. The Classification Performance of a Three-Product Cyclone. *Wirel. Pers. Commun.* **2018**, *103*, 55–68. [[CrossRef](#)]
12. Vieira, L.G.M.; Damasceno, J.J.R.; Barrozo, M.A.S. Improvement of hydrocyclone separation performance by incorporating a conical filtering wall. *Chem. Eng. Process. Process Intensif.* **2010**, *49*, 460–467. [[CrossRef](#)]
13. Silva, N.K.G.; Silva, D.O.; Vieira, L.G.M.; Barrozo, M.A. Effects of underflow diameter and vortex finder length on the performance of a newly designed filtering hydrocyclone. *Powder Technol.* **2015**, *286*, 305–310. [[CrossRef](#)]
14. Ghodrat, M.; Kuang, S.B.; Yu, A.B.; Vince, A.; Barnett, G.D.; Barnett, P.J. Numerical analysis of hydrocyclones with different conical section designs. *Miner. Eng.* **2014**, *62*, 74–84. [[CrossRef](#)]
15. Patra, G.; Velpuri, B.; Chakraborty, S.; Meikap, B.C. Performance evaluation of a hydrocyclone with a spiral rib for separation of particles. *Adv. Powder Technol.* **2017**, *28*, 3222–3232. [[CrossRef](#)]
16. Yang, Q.; Wang, H.L.; Liu, Y.; Li, Z.M. Solid/liquid separation performance of hydrocyclones with different cone combinations. *Sep. Purif. Technol.* **2010**, *74*, 271–279. [[CrossRef](#)]
17. Chang, Y.L.; Wang, H.L.; Jin, J.H.; Liu, Z.M.; Lv, W.J. Flow distribution and pressure drop in UZ-type mini-hydrocyclone group arranged in compact parallel manifolds. *Exp. Therm. Fluid Sci.* **2019**, *100*, 114–123. [[CrossRef](#)]
18. Jiang, L.; Liu, P.; Yang, X.; Zhang, Y.; Li, F. Comparative classification studies of red mud by using hydrocyclones. *Miner. Eng.* **2019**, *131*, 124–130. [[CrossRef](#)]
19. Liu, S.; Zhang, D.; Xu, J.Y. Breakup and coalescence regularity of non-dilute oil drops in a vane-type swirling flow field. *Chem. Eng. Res. Des.* **2018**, *129*, 35–54. [[CrossRef](#)]
20. Ye, J.; Xu, Y.; Song, X.; Yu, J. Novel conical section design for ultra-fine particles classification by a hydrocyclone. *Chem. Eng. Res. Des.* **2019**, *144*, 135–149. [[CrossRef](#)]
21. Jiang, L.; Liu, P.; Zhang, Y.; Wang, H.; Gui, X. Design boundary layer structure for improving the particle separation performance of a hydrocyclone. *Powder Technol.* **2019**, *350*, 1–14. [[CrossRef](#)]
22. Zou, J.; Wang, C.X.; Ji, C. Experimental study on the air core in a hydrocyclone. *Dry. Technol.* **2016**, *34*, 854–860. [[CrossRef](#)]
23. Razmi, H.; Soltani, G.A.; Mohebbi, A. CFD simulation of an industrial hydrocyclone based on multiphase particle in cell (MPPIC) method. *Sep. Purif. Technol.* **2019**, *209*, 851–862. [[CrossRef](#)]
24. Cui, B.; Zhang, C.; Wei, D.; Lu, S.; Feng, Y. Effects of feed size distribution on separation performance of hydrocyclones with different vortex finder diameters. *Powder Technol.* **2017**, *322*, 114–123. [[CrossRef](#)]
25. Guizani, R.; Mhiri, H.; Bournot, P. Effects of the geometry of fine powder outlet on pressure drop and separation performances for dynamic separators. *Powder Technol.* **2017**, *314*, 599–607. [[CrossRef](#)]
26. Sindall, R.C.; Dapelo, D.; Leadbeater, T.; Bridgeman, J. Positron emission particle tracking (PEPT): A novel approach to flow visualisation in lab-scale anaerobic digesters. *Flow Meas. Instrum.* **2017**, *54*, 250–264. [[CrossRef](#)]
27. Wang, J.; Bai, Z.; Yang, Q.; Fan, Y.; Wang, H. Investigation of the simultaneous volumetric 3-component flow field inside a hydrocyclone. *Sep. Purif. Technol.* **2016**, *163*, 120–127. [[CrossRef](#)]
28. Pérez, D.; Cornejo, P.; Rodríguez, C.; Concha, F. Transition from spray to roping in hydrocyclones. *Miner. Eng.* **2018**, *123*, 71–84. [[CrossRef](#)]
29. Gong, H.; Yu, B.; Dai, F.; Peng, Y.; Shao, J. Simulation on performance of a demulsification and dewatering device with coupling double fields: Swirl centrifugal field and high-voltage electric field. *Sep. Purif. Technol.* **2018**, *207*, 124–132. [[CrossRef](#)]
30. Wang, X.; Wang, S.; Tian, R.; Wang, R.; Liu, L.; Sun, Q.; Fan, J. Numerical study on flow behavior of multi-component particles in a fluidized bed using a TFM-DEM hybrid model. *Powder Technol.* **2018**, *338*, 795–805. [[CrossRef](#)]

31. Yang, Q.; Lv, W.J.; Ma, L.; Wang, H.L. CFD study on separation enhancement of mini-hydrocyclone by particulate arrangement. *Sep. Purif. Technol.* **2013**, *102*, 15–25. [[CrossRef](#)]
32. Pei, B.; Liu, Y.; Dong, K.; Jiang, Y.; Du, X.; Wang, B. The effect of cross-shaped vortex finder on the performance of cyclone separator. *Powder Technol.* **2017**, *313*, 135–144. [[CrossRef](#)]
33. Delgadillo, J.A.; Rajamani, R.K. Exploration of hydrocyclone designs using computational fluid dynamics. *Int. J. Miner. Process.* **2007**, *84*, 252–261. [[CrossRef](#)]
34. Ghodrat, M.; Qi, Z.; Kuang, S.B.; Ji, L.; Yu, A.B. Computational investigation of the effect of particle density on the multiphase flows and performance of hydrocyclone. *Miner. Eng.* **2016**, *90*, 55–69. [[CrossRef](#)]
35. Narasimha, M.; Brennan, M.S.; Holtham, P.N. CFD modeling of hydrocyclones: Prediction of particle size segregation. *Miner. Eng.* **2012**, *39*, 173–183. [[CrossRef](#)]
36. Jiang, L.; Liu, P.; Zhang, Y.; Yang, X.; Wang, H. The Effect of Inlet Velocity on the Separation Performance of a Two-Stage Hydrocyclone. *Minerals* **2019**, *9*, 209. [[CrossRef](#)]
37. Yang, X.; Simmons, M.J.; Liu, P.; Zhang, Y.; Jiang, L. Effect of feed body geometry on separation performance of hydrocyclone. *Sep. Sci. Technol.* **2018**, *54*, 2959–2970. [[CrossRef](#)]
38. Chu, K.W.; Wang, B.; Yu, A.B.; Vince, A. CFD-DEM modelling of multiphase flow in dense medium cyclones. *Powder Technol.* **2009**, *193*, 235–247. [[CrossRef](#)]
39. He, F.; Zhang, Y.; Wang, J.; Yang, Q.; Wang, H.; Tan, Y. Flow Patterns in Mini-Hydrocyclones with Different Vortex Finder Depths. *Chem. Eng. Technol.* **2013**, *36*, 1935–1942. [[CrossRef](#)]
40. Slack, M.D.; Prasad, R.O.; Bakker, A.; Boysan, F. Advances in Cyclone Modelling Using Unstructured Grids. *Chem. Eng. Res. Des.* **2000**, *78*, 1098–1104. [[CrossRef](#)]



© 2020 by the authors. Licensee MDPI, Basel, Switzerland. This article is an open access article distributed under the terms and conditions of the Creative Commons Attribution (CC BY) license (<http://creativecommons.org/licenses/by/4.0/>).